CASSCF Investigation of Electronic Excited States of 2-Aminopurine

Edward L. Rachofsky,[†] J. B. Alexander Ross,[†] Morris Krauss,[‡] and Roman Osman*[,§]

Departments of Biochemistry and Molecular Biology and Physiology and Biophysics, Mount Sinai School of Medicine, One Gustave L. Levy Place, New York, New York 10029, and Center for Advanced Research in Biotechnology, National Institute of Standards and Technology, 9600 Gudelsky Drive, Rockville Maryland 20850

Received: July 6, 2000

2-Aminopurine is a highly fluorescent analogue of adenine that can be incorporated synthetically into DNA with little perturbation of the native double-helical structure. The sensitive dependence of the quantum yield of this fluorophore on nucleic acid conformation has made it an invaluable probe of DNA structure, dynamics, and interactions. To assist in the development of models for the molecular interpretation of fluorescence measurements, the electronic structure of 2-amino-9-methylpurine has been calculated in the ground state and the lowest singlet $\pi\pi^*$ and $n\pi^*$ excited states. These computations employed the complete active space multiconfigurational self-consistent field method (CASSCF), supplemented by multiconfigurational quasi-degenerate perturbation theory (MCQDPT). The predicted energies for $\pi\pi^*$ excitation and emission and $n\pi^*$ excitation are in good agreement with previous experimental values. The permanent molecular dipoles of the ground and $\pi\pi^*$ excited states are similar in magnitude and direction, consistent with experimental observations of weak solvatochromic shifts in $\pi\pi^*$ absorption and emission spectra. However, the permanent dipole of the $n\pi^*$ state is rotated approximately 60° relative to that of the ground state, implying that the $n\pi^*$ excitation energy will increase in more polar solvents due to the relative destabilization of this state by unfavorably oriented solvent dipoles. This result demonstrates that the "blue-shift" of the $n\pi^*$ state in polar solvents, which is commonly attributed to the effect of hydrogen bonding, can arise entirely from a general solvent effect. The energy of a radiationless vibronic transition from the $\pi\pi^*$ state to the $n\pi^*$ state will increase in more polar solvents, provided that the solvent does not rearrange during the transition. Consequently, the efficiency of fluorescence quenching by vibronic coupling between the $\pi\pi^*$ and $n\pi^*$ states is predicted to decrease significantly in such solvents. The geometry of the fluorescent emitting state, obtained by CASSCF optimization of the $\pi\pi^*$ state, is moderately buckled due to the occupation of an antibonding orbital localized to C6. This buckling implies an out-of-plane vibration during the relaxation of the $\pi\pi^*$ state, which is required for vibronic coupling between this state and the $n\pi^*$ state. Such a solvent-sensitive intramolecular quenching mechanism may account for the observed dependence of the fluorescence lifetime of 2-aminopurine on the local environment both in pure solvents and in DNA.

Introduction

The standard purine and pyrimidine bases of nucleic acids, unlike the aromatic amino acids tyrosine and tryptophan that are naturally found in proteins, show negligible fluorescence emission.[3] Consequently, fluorescence studies of DNA and RNA require that these macromolecules be labeled with an extrinsic fluorophore. 2-Aminopurine (2AP) is a highly fluorescent isomer of adenine, with spectroscopic and structural properties that make it a convenient probe for studies of nucleic acid structure and function. The lowest-energy absorption band of 2AP in solution is found at wavelengths longer than those of the natural nucleotides and aromatic amino acids, enabling selective excitation of this fluorophore from samples containing both proteins and DNA or RNA. The structure of oligonucleotides is minimally perturbed by the incorporation of 2AP, which forms a stable Watson−Crick base pair with thymine.[9,21] The fluorescence of 2AP is strongly quenched within double-helical DNA and is sensitive to changes in DNA structure. This sensitivity to the local environment has been employed to study biochemical processes such as nucleotide addition by Klenow DNA polymerase,[6] base flipping by the repair enzyme uracil DNA glycosylase,[23] and formation of the open complex of *Escherichia coli* RNA polymerase.[24]

Despite the wide utilization of 2AP fluorescence for biochemical and biophysical studies, the effects of intermolecular interactions on its emission energy, intensity decay kinetics, and quantum yield are poorly understood. Within a DNA strand, the fluorophore experiences a complex environment and participates in several noncovalent interactions, including hydrogen bonding and aromatic stacking. Understanding the effects of each of these interactions on the photophysics of 2AP would enable a more detailed molecular interpretation of spectroscopic changes in relation to the structure and dynamics of DNA.

A description of the electronic structure of this fluorophore in the ground and excited states is essential to the development of such mechanistic models. To this end, we have performed

* Corresponding author. Tel.: (212) 241-5609. Fax: (212) 860-3369. Email: osman@inka.mssm.edu.

[†] Department of Biochemistry and Molecular Biology, Mount Sinai School of Medicine.

[‡] Center for Advanced Research in Biotechnology, National Institute of Standards and Technology.

[§] Department of Physiology and Biophysics, Mount Sinai School of Medicine.

10.1021/jp002413s CCC: $20.00
Published on Web 12/01/2000

ab initio quantum chemical calculations of 2-amino-9-methylpurine (2A9MP) in the electronic ground state and the lowest singlet $\pi\pi^*$ and $n\pi^*$ excited states. These calculations employed the complete active space self-consistent field[18] (CASSCF) method, supplemented by multiconfigurational quasi-degenerate perturbation theory[16] (MCQDPT) and were performed with large active spaces containing the full π electronic manifold and several σ orbitals.

Several previous theoretical and experimental studies of 2AP have attempted to assign electronic transitions to the observed absorption spectrum.[1,10,12,20] A consensus has emerged from this literature that the lowest-energy absorption band in solution represents a single $\pi\pi^*$ transition centered at approximately 4.11 eV (302 nm). The maximum of the absorption spectrum is fairly insensitive to the solvent environment, varying no more than 0.1 eV over a wide range of solvents.[5,20] The fluorescence emission, which occurs from the same $\pi\pi^*$ state, is subject to somewhat greater solvatochromic shifts, ranging from 3.60 eV (344 nm) for 2-amino-9-ethylpurine (2A9EP) in cyclohexane to approximately 3.35 eV (370 nm) for 2AP and various derivatives in neutral aqueous buffer.[5,20,25] The emission energy generally decreases with increasing solvent polarity, implying that the emitting state is more polar than the ground state. This trend is consistent with a general solvent effect arising from dipolar interactions that stabilize the more polar emitting state better than the ground state. In addition, the fluorescence quantum yield increases dramatically with increasing solvent polarity.[20,25] The solvent dependence of the quantum yield suggests the presence of an intramolecular quenching mechanism that is sensitive to the energy of the emitting state. It has been hypothesized that this solvent-dependent quenching arises from vibronic coupling between the $\pi\pi^*$ emitting state and a nearby $n\pi^*$ state, which would result in nonradiative decay of the excitation because it increases the probability of radiationless vibrational transition between the $\pi\pi^*$ and ground states.[20] The solvent dependence of this mechanism has been proposed to arise from a difference in the magnitudes of the permanent dipoles of the $\pi\pi^*$ and $n\pi^*$ states, which would impart a differential sensitivity to dipolar (general solvent) interactions.[1] Alternatively, it has been hypothesized that this trend represents the destabilization of the $n\pi^*$ state by hydrogen bonding (the "$n\pi^*$ blue-shift" effect), where the energy of the destabilizing hydrogen bond increases with solvent polarity.[20] Recently, the presence of such an $n\pi^*$ transition at approximately 4.5 eV was inferred from features of the linear dichroism and fluorescence anisotropy excitation spectra of 2AP.[10]

Vibronic coupling between excited electronic states depends on two factors.[13,26] First, the energy difference between the states must be reasonably small because the probability of vibronic coupling depends approximately inversely on this energy gap. Therefore, the efficiency of this process will vary with any factor, such as solvation, that perturbs the state energies. Second, there must be an appropriately oriented vibrational mode that can increase the transition probability between the two states. For coupling between the $\pi\pi^*$ and $n\pi^*$ states of a planar aromatic molecule, the vibrational mode must be directed out of the molecular plane because the states belong to different symmetries. Vibronic coupling between $\pi\pi^*$ and $n\pi^*$ states results in efficient quenching of $\pi\pi^*$ fluorescence because the frequency of the vibronically active mode of the $\pi\pi^*$ state decreases, increasing the Franck−Condon factor for the radiationless decay of $\pi\pi^*$ excitation.[13] Thus, vibronic coupling provides an intramolecular mechanism of fluorescence quenching that is also solvent-sensitive due to its dependence on the energy difference between the states.

The present calculations seek to evaluate the hypothesis that the solvent dependence of the quantum yield of 2AP arises from vibronic coupling between the emitting $\pi\pi^*$ state and a nearby $n\pi^*$ state, with the efficiency of this intramolecular quenching pathway modulated by solvent-induced shifts in the energies of the two states. The electronic structures of the lowest singlet $\pi\pi^*$ and $n\pi^*$ states are computed by CASSCF with large active spaces. The effects of solvent polarity on the energies of excitation to these states are evaluated from their permanent molecular dipoles using a classical model of solvation.[4,15] The geometry of the $\pi\pi^*$ state is optimized to obtain the fluorescent emitting state, and the significance of out-of-plane vibrations in excited-state relaxation is determined. The results are consistent with the hypothesis that vibronic coupling to the $n\pi^*$ state quenches the $\pi\pi^*$ fluorescence of 2AP. Furthermore, it is demonstrated that the observed solvent dependence of this process can be rationalized within the framework of a simple classical model of dipolar interactions.

Calculation Methods

All molecular orbital calculations were performed using the GAMESS program package.[19] The 6-31G* basis set was employed, and core orbitals were approximated using the SBK effective core potentials for heavy atoms.[22] The 9-methyl derivative of 2AP was chosen for these calculations because it is essentially isoelectronic with the 9-ribosylated and deoxyribosylated derivatives found in nucleic acids. Substitution at the 9-position also eliminates the complications associated with tautomerism between the 7-H and 9-H forms of 2AP, which has been shown to significantly alter the calculated electronic states of the chromophore.[10]

Geometries. The ground-state geometry was optimized using the second-order Møller−Plesset (MP2) perturbation method under the assumption of planar (C_s) symmetry. However, for optimization of the $\pi\pi^*$ state, the geometry was permitted to assume C_1 symmetry. In this calculation, the symmetry of the ground-state geometry (the starting structure for excited-state optimization) was removed by manually rotating the methyl protons by 90° around the N9−C9′ bond. This perturbation did not significantly alter the properties of the calculated electronic states (Table 1) and was applied only to assist in the convergence of CASSCF. The geometry of the lowest singlet $\pi\pi^*$ excited state was optimized by the CASSCF gradient using an active space consisting of 14 electrons in 2 σ, 5 π, and 3 π^* orbitals. All occupied π orbitals were included in the active space, except for one localized to the N9−C9′ bond, which was excluded because excitations from this orbital did not significantly contribute to the electronic configuration at the initial geometry. Coordinates are available upon request.

Electronic Structures and Energies. The active spaces, geometries, and electronic states for all CASSCF calculations reported here are summarized in Table 1. The electronic wave functions and energies for the ground state and lowest singlet $\pi\pi^*$ and $n\pi^*$ excited states were computed by CASSCF at the ground-state geometry (Franck−Condon states) to obtain excitation energies, and the ground and $\pi\pi^*$ states were calculated at the optimized $\pi\pi^*$ geometry to obtain the emission energy. The active space for ground-state and $n\pi^*$ state calculations consisted of 20 electrons in 5 σ, 5 π, 2 π^*, and 1 σ^* orbitals. However, for $\pi\pi^*$ state calculations, the active space was reduced to 14 electrons in 2 σ, 5 π, and 3 π^* orbitals (the same as those for geometry optimization) to improve convergence. To determine

TABLE 1: Summary of CASSCF Calculations

no.	state	geometry	active space	E_{CASSCF} (a.u.)	E_{MCQDPT} (a.u.)
1	ground	ground	$20e^-/5\sigma,5\pi,2\pi^*,1\sigma^*$	−85.470762	−86.869352
2	ground	ground[a]	$20e^-/5\sigma,5\pi,2\pi^*,1\sigma^*$	−85.473134	−
3	ground	ground[a]	$14e^-/2\sigma,5\pi,3\pi^*$	−85.463073	−
4	ground	$\pi\pi^*$	$20e^-/5\sigma,5\pi,2\pi^*,1\sigma^*$	−85.450222	−
5	ground	$\pi\pi^*$	$14e^-/2\sigma,5\pi,3\pi^*$	−85.450391	−
6	$\pi\pi^*$	ground[a]	$14e^-/2\sigma,5\pi,3\pi^*$	−85.270408	−
7	$\pi\pi^*$	$\pi\pi^*$	$14e^-/2\sigma,5\pi,3\pi^*$	−85.292745	−
8	ground/$\pi\pi^*$[b]	ground[a]	$20e^-/5\sigma,5\pi,2\pi^*,1\sigma^*$	−85.459631/−85.247757	−86.886173/−86.740178
9	ground/$\pi\pi^*$[b]	$\pi\pi^*$	$20e^-/5\sigma,5\pi,2\pi^*,1\sigma^*$	−85.448126/−85.293174	−86.867993/−86.733001
10	$n\pi^*$	ground	$20e^-/5\sigma,5\pi,2\pi^*,1\sigma^*$	−85.256192	−86.688564

[a] Ground-state geometry with C9′ methyl rotation. [b] Equally weighted state-averaged wave function.

the effect of active space on computed molecular properties such as dipole moment, we also calculated the ground state using this reduced active space at both excitation and emission geometries. The CASSCF energy of $n\pi^*$ excitation was obtained from the difference between the energies of wave functions computed for the pure ground and $n\pi^*$ states. However, the energies of $\pi\pi^*$ excitation and emission were computed from state-averaged wave functions in which the ground and $\pi\pi^*$ states were equally weighted. State averaging has been shown to be an effective method of equalizing the contribution of dynamic electron correlation to the ground- and excited-state energies.[11] The active space for the state-averaged calculations consisted of 20 electrons in 5 σ, 5 π, 2 π^* and 1 σ^* orbitals. Thus, all transition energies were obtained from CASSCF calculations with an active space consisting of 20 electrons in 13 orbitals, although $n\pi^*$ energies were determined for pure-state wave functions and $\pi\pi^*$ energies for state-averaged wave functions.

To obtain more accurate transition energies between the ground and $\pi\pi^*$ states, MCQDPT was applied to the state-averaged CASSCF wave functions. The same active space was employed for multiconfigurational perturbation as for the corresponding state-averaged CASSCF. For correction of the excitation energy for the $n\pi^*$ state, MCQDPT was separately applied to the pure wave functions of the ground and $n\pi^*$ states.

Molecular orbitals were plotted using the program MOLDEN (Center for Molecular and Biomolecular Informatics, University of Nijmegen, The Netherlands).

Solvatochromic Shifts. The directions and relative magnitudes of solvatochromic shifts in electronic spectra were predicted using elements of a simplified classical theory.[4,15] In this model, the solvated fluorophore is represented as a point dipole occupying a cavity of radius a within a continuum solvent of dielectric constant ϵ and refractive index n. This model excludes specific chemical interactions, such as hydrogen bonding, between the fluorophore and solvent molecules. The energy shifts of solvation in absorption and emission spectra relative to the vacuum depend on the properties of the solvent according to

$$\Delta E = \frac{1}{a^3}\left\{A\left(\frac{\epsilon-1}{\epsilon+2}-\frac{n^2-1}{n^2+2}\right)+B\left(\frac{n^2-1}{2n^2+1}\right)\right\} \quad (1)$$

The coefficients A and B depend on the properties of the fluorophore and are given by

$$A_{abs,em} = \vec{\mu}_{g,e}(\vec{\mu}_g - \vec{\mu}_e) \quad (2)$$

$$B = (\mu_g{}^2 - \mu_e{}^2) \quad (3)$$

where μ_g and μ_e are the ground- and excited-state molecular dipoles, respectively. The first and second terms in eq 1 represent electrostatic interactions of the fluorophore with the permanent and induced dipoles of the solvent, respectively. Although the two terms in eq 1 are similar in magnitude, the factor multiplied by A varies over a much wider range between solvents than that multiplied by B. For example, when the solvent is changed from 1,4-dioxane to water, the factor multiplied by A changes from 0.03 to 0.76, whereas the factor multiplied by B changes from 0.20 to 0.17. Thus, the extent of the predicted solvatochromic shift of an electronic transition depends on the differences in both magnitude and direction of the permanent molecular dipoles for the two states involved and on the dielectric and optical properties of the solvent.

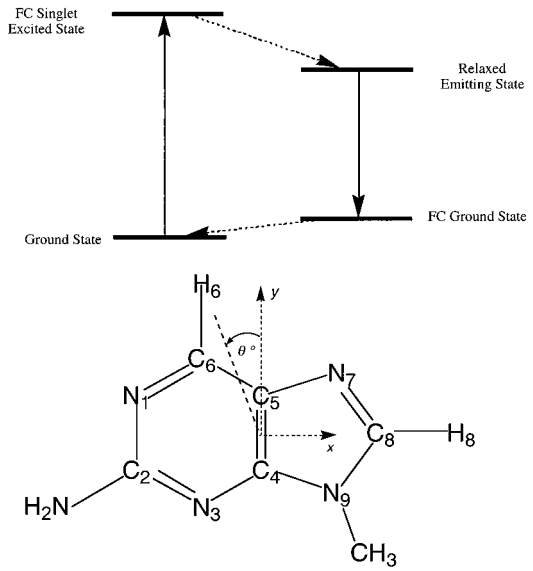

Figure 1. (A) Jabłoński diagram for the excitation and emission of the lowest singlet $\pi\pi^*$ state of 2AP. The solid arrows represent the absorption or emission of a photon. The dashed arrows represent the vibrational relaxation of the Franck−Condon (FC) state. (B) Axes and numbering conventions for 9M2AP.

Results

The ab initio molecular orbital calculations presented below recapitulate the cycle of electronic excitation and fluorescence emission of 2A9MP as it is schematically presented in Figure 1a. The molecular geometry was first optimized in the ground state. At this geometry, the lowest singlet $\pi\pi^*$ excited state was calculated, and the energy and transition dipole of the first ultraviolet absorption were predicted. The geometry of this excited state was optimized to obtain the fluorescent emitting state. Finally, the ground state was recalculated at the emitting geometry to obtain the energy and transition dipole of fluorescence emission. The effects of solvation on the absorption and emission spectra were calculated from the properties of these

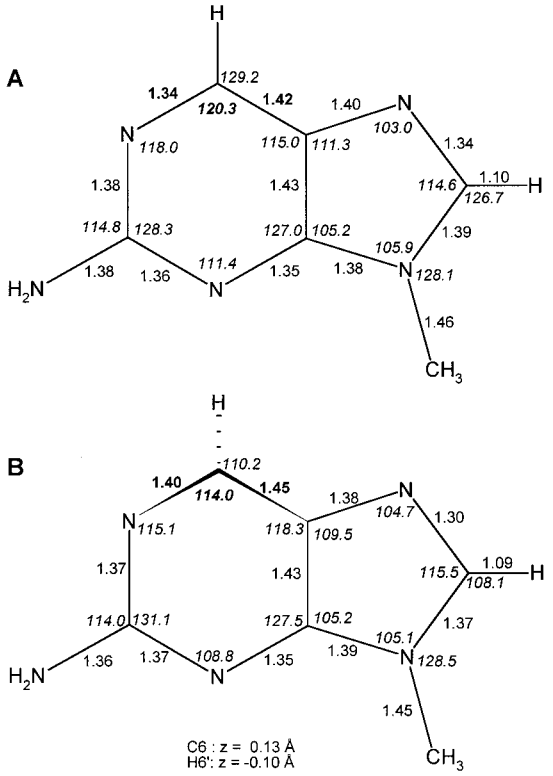

Figure 2. Optimized geometry of 2A9MP in (A) the electronic ground state and (B) the $\pi\pi^*$ emitting state. Bond distances are indicated in normal type, and angles in italics. Bold-faced numbers indicate values that differ significantly between ground-state and $\pi\pi^*$ geometries.

four states. In addition, the lowest singlet $n\pi^*$ excited state was calculated and the energy of excitation to this state predicted.

The numbering and coordinate conventions for 2A9MP are shown in Figure 1b. The *x*-axis is defined as the line passing through C8 and bisecting the N1−C2 bond. The *y*-axis is approximately parallel to the C4−C5 bond. Angles in the molecular plane are defined with respect to the *y*-axis, with a positive deflection resulting from a counterclockwise rotation, as shown in Figure 1b.

Ground-State Geometry and Absorption Spectrum. The bond distances and angles for the MP2/6-31G* ground-state geometry of 2A9MP are depicted in Figure 2. These values agree well with the 2AP geometry previously calculated using the same method and basis set[2] and with the geometry for the 2AP moiety in the crystal structure of the antiviral drug famcyclovir.[8]

The total energies for all computed electronic states are listed in Table 1, and the predicted energies and transition dipoles for $\pi\pi^*$ excitation and emission and for $n\pi^*$ excitation are summarized in Table 2. No vapor-phase or low-temperature spectra exists for 2AP or its derivatives, so calculated transition energies can only be validated by comparison with solution spectra. The CASSCF transition energies are consistently greater than the experimental values. These overestimates are typical of CASSCF calculations of the spectra of aromatic chromophores because this method does not fully account for dynamic electron correlation.[18] The MCQDPT energies of the same transitions show significantly better agreement with experimental values than the respective CASSCF energies. The MCQDPT energy of $\pi\pi^*$ excitation is 3.97 eV (corresponding to a wavelength of 312 nm), which differs by less than 0.11 eV from the experimental maxima (3.99−4.08 eV)[5,20,25] of the first absorption band in a variety of solvents.

TABLE 2: Transition Energies and Dipoles for Singlet $\pi\pi^*$ and $n\pi^*$ States

transition	E_{MCSCF} (eV)	E_{MCQDPT} (eV)	E_{expt} (eV)	θ^a	ssc. strength
$S_0 \rightarrow \pi\pi^*$	5.76 [215][b,c]	3.97 [312]	4.06[e] [306]	110°	0.615
$S_0 \rightarrow n\pi^*$	5.84 [212][d]	4.91 [252]	4.46[f] [278]	–	–
$\pi\pi^* \rightarrow S_0$[g]	4.22 [294][c]	3.67 [338]	3.60[h] [344]	113°	0.113

[a] Transition dipole. [b] Transition energy (eV) and [wavelength (nm)]. [c] Transition energy calculated from equally weighted state-averaged wave function with an active space of 20 electrons in 13 orbitals. [d] Transition energy calculated from pure-state wave functions, each with an active space of 20 electrons in 13 orbitals. [e] Absorption maximum in ethyl ether (ref 13). [f] Estimated absorption maximum in neutral aqueous buffer (ref 12). [g] Emission calculated at optimized $\pi\pi^*$ geometry. [h] Emission maximum in cyclohexane (ref 14).

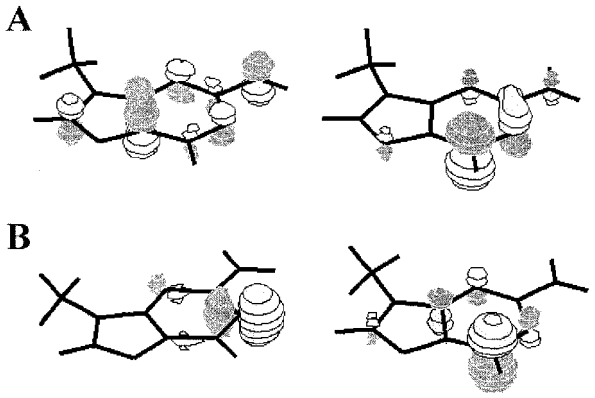

Figure 3. Molecular orbital p_z coefficients for orbitals involved in electronic transitions at the ground-state geometry. (A) Orbitals involved in $\pi\pi^*$ excitation, and (B) orbitals involved in nπ^* excitation. For each transition, the largest coefficient in the configurational expansion is for a single excitation from the molecular orbital depicted on the left to the one shown on the right.

The electronic configuration of the $\pi\pi^*$ state is composed predominantly of a small number of states, which are listed in Table 3. The largest coefficient is for a configuration representing a single excitation from the highest occupied (HOMO) to the lowest unoccupied (LUMO) molecular orbital. The p_z coefficients of these two orbitals at the ground-state geometry are depicted in Figure 3a. The HOMO is a highly delocalized π orbital, with the greatest densities on the C4−C5 bond, a diffuse π system on N3−C2−N1−C6, and localized p_z orbitals on C8 and the extracyclic amino group. The LUMO is a π^* orbital localized almost entirely to C6 and the N1−C2 π bond. Thus, excitation results in a shift of electron density from the C4−C5 bond and the delocalized four-center π bond to C6. Except for a relatively small loss of electron density on C8, the imidazole ring is not involved in the excitation. No σ excitation makes a significant contribution to the CASSCF wave function. Optimization of the excited-state geometry (see below) does not qualitatively alter this orbital configuration.

At both the ground-state and excited-state geometries, one of the five σ orbitals initially included in the active space changes in character to a π orbital during CASSCF optimization. In addition, at the emitting geometry, the active σ^* orbital takes on the character of a π^* orbital. These changes reflect the coupling between the σ and π manifolds that is achieved with a mixed active space. However, neither the π nor the π^* orbital that rotates into the active space during CASSCF participates significantly in the electronic excitation.

The CASSCF energy for excitation to the lowest singlet $n\pi^*$ state is 5.84 eV (212 nm), and the corresponding MCQDPT energy is 4.91 eV (252 nm). The latter result is in reasonably

TABLE 3: Configurational States Involved in Electronic Transitions[a]

$\pi\pi^*$ excitation		$\pi\pi^*$ emission		nπ^* excitation	
coefficient	$\sigma\pi\sigma\sigma\pi\pi\pi\pi\pi$ $\pi\pi\sigma^*$	coefficient	$\sigma\sigma\pi\sigma\sigma\pi\pi\pi\pi\pi$ $\pi\pi\pi^*$	coefficient	$\sigma\sigma\pi\sigma\sigma\pi\pi\pi\pi\sigma$ $\pi\pi\sigma^*$
0.78	2222222221 100	0.59	2222222221 010	0.75	2222222221 100
−0.32	2222222212 100	−0.45	2222222221 100	0.41	2222122222 100
0.30	2222222221 010	0.23	2222222211 110	−0.32	2222222221 010
0.21	2222221222 100	0.16	2222222212 010	0.17	2221222222 100
−0.14	2222222212 010	−0.15	2222222212 001	−0.17	2222122222 010
0.12	2222221221 110	0.14	2222222211 020	0.11	2222222121 200
0.12	2222221221 200	−0.14	2222221221 110	−0.11	2222221221 200
0.10	2222222220 200	0.13	2222212222 010		
		0.13	2222212221 110		
		0.11	2222221222 010		
		−0.11	2222221222 001		

[a] Including only the 10 bonding and 3 antibonding orbitals in the active space. Note that the order of the orbitals is not the same for $\pi\pi^*$ and $n\pi^*$ excitations. Bonding and antibonding orbitals are separated by a space.

good agreement with the experimental value of 4.46 eV (278 nm) in neutral aqueous buffer,[10] which is highly uncertain due to the low oscillator strength and extensive solution spectral broadening characteristic of $n\pi^*$ transitions. State averaging was not employed in the determination of these energies due to the differing symmetries of the ground and $n\pi^*$ states.

As with the $\pi\pi^*$ state, the $n\pi^*$ state is dominated by a few configurational state functions, as listed in Table 3. The largest coefficient is for a configuration representing a single excitation from a nonbonding orbital of A' symmetry localized on N1 to an A'' antibonding orbital localized on C6. The distribution of this singly occupied π^* orbital is very similar to that of the corresponding orbital in the $\pi\pi^*$ state. These orbitals are depicted in Figure 3b.

Excited-State Geometry and Emission Spectrum. The geometry of the lowest singlet $\pi\pi^*$ excited state was optimized by the CASSCF gradient with an active space consisting of 14 electrons in 2 σ, 5 π, and 3 π^* orbitals. The 2 σ orbitals had the character of nonbonding orbitals localized to N1 and N3. This active space was generated by removing 3 σ orbitals and 1 σ^* orbital from the active space used for electronic structure calculations. Reduction of the active manifold was required to permit excited-state optimization with reasonable demands on computational resources. The $\pi\pi^*$ excitation energy (Table 2) was effectively unchanged by reduction of the active space.

The bond distances, angles, and selected dihedral angles for the excited-state geometry are depicted in Figure 2. The differences between this geometry and the ground state parallel the changes in electron density upon excitation. In the excited state, the C6−N1 and C5−C6 bond distances are increased, and the adjacent N1−C2 and C5−N7 bonds are correspondingly shortened. The increased separation between C6 and its neighbors is consistent with a decrease in bond order due to occupation of the LUMO, an antibonding orbital localized to C6. This separation is accompanied by a modest (0.13 Å) buckling of C6 out of the molecular plane and an approximately equal and opposite (−0.10 Å) displacement of H6. Buckling of the pyrimidine ring is consistent with mixing between the σ and π electronic manifolds, as expected when both types of orbitals are present in the active space. A similar optimization with an active space containing no σ orbitals produced a planar geometry (data not shown), indicating the importance of coupling the σ and π manifolds in the active space for geometry optimization. The observed buckling of the optimized $\pi\pi^*$ geometry implies excitation of an out-of-plane vibrational mode during relaxation of the excited state. Such an extraplanar vibration is consistent with the previously hypothesized mechanism of fluorescence quenching by vibronic coupling to a nearby $n\pi^*$ state.[20]

The observed buckling of the $\pi\pi^*$ state does not agree with previously reported results for the excited-state geometry of 2AP, which was found to be essentially planar by three methods: semiempirical AM1, CIS, and CASSCF with an active space consisting of 4 π electrons in 4 orbitals.[1] In this previous study, it was also reported that the amino H-atoms of N2′ rotated 90° out of the molecular plane; this rotation is not observed in the current geometry. The disparity between these results is attributable to several improvements in methodology in the present study. In the present calculations, the use of polarization functions improves the description of wave functions. More importantly, a much larger active space containing both σ and π orbitals permits the $\pi\pi^*$ state to attain a puckered conformation. Such a geometry cannot be achieved with a π-only active space.

As with the excitation energies, the CASSCF energy of fluorescence emission is significantly greater than experimental values. However, inclusion of electron correlation through perturbation theory improves the results considerably. The MCQDPT emission energy is 3.67 eV (338 nm), in excellent agreement with the experimental emission maxima of 3.60 eV (344 nm) for 9E2AP in cyclohexane.[25]

The CASSCF wave function of the $n\pi^*$ state could not be converged at the optimized $\pi\pi^*$ geometry. Without molecular symmetry, it is not possible to restrict the configurational expansion to A'' states, and none of the 20 lowest-energy excited states obtained from CI expansion of the initial orbitals were found to have even approximate A'' character. However, optimization of the $\pi\pi^*$ state is predicted to decrease the energy of the $n\pi^*$ state by approximately the same amount as that of the $\pi\pi^*$ state (∼0.5 eV), given the similar distributions of electron density in the two states (see Figure 3). Therefore, qualitative conclusions about the properties of the $n\pi^*$ state at the emitting geometry can be inferred from the wave function computed at the ground-state geometry.

Permanent Molecular Dipoles and Solvatochromic Shifts. The permanent molecular dipoles in the ground state and the $\pi\pi^*$ and $n\pi^*$ excited states are shown in Figure 4. Each of these dipoles was computed from the wave function of the pure electronic state. Reduction of the active space from 20 to 14 electrons (see Table 1) has a negligible effect on the molecular dipole of the ground state: the magnitude decreases less than 5%, and the direction changes by less than 10°. The same consistency may not be evident for the excited states, which will probably depend more sensitively on the composition of the active space. However, we will compare the dipoles of the ground and $n\pi^*$ states (computed with 20 electrons in 13 active orbitals) with that of the $\pi\pi^*$ state (computed with 14 electrons in 10 active orbitals) directly, under the assumption that the

TABLE 4: Solvatochromic Shift Coefficients

transition	$\|\mu_1\|$, $\|\mu_2\|$ (D)[a]	A (D^2)	B (D^2)	A/a^3 (eV)[b]	B/a^3 (eV)[b]	E_0 (eV)[b]	a (Å)[b]	E_{wat} (eV)[c]
$S_0 \rightarrow \pi\pi^*$	3.64, 4.68	−2.4	−8.6	−0.06	−0.22	4.11	2.91	4.07
$S_0 \rightarrow n\pi^*$	3.67, 4.49	5.4	−6.7	0.51	−0.64	–	–	–
$\pi\pi^* \rightarrow S_0$	4.33, 3.68	−3.7	−5.2	−0.35	−0.50	3.70	1.87	3.36
$\pi\pi^* \rightarrow n\pi^*$[d]	4.68, 4.49	4.8	1.6	0.51	−0.64	–	–	–

[a] Dipole moments of the two states involved in the transition. [b] Calculated from a least-squares fit of the experimental transition energies from refs 11, 14, and 15 to eq 1. The permanent molecular dipoles of the ground and $\pi\pi^*$ states were fixed to the values obtained from CASSCF for this analysis, and the vacuum transition energy E_0 and the cavity radius a were taken as adjustable parameters. For the $\pi\pi^*$ state, excitation and emission data were fitted separately. For the $n\pi^*$ state, the reported solvent shift energies are calculated from the permanent dipole of the $n\pi^*$ state and from the values of E_0 and a calculated for the $\pi\pi^*$ emission. [c] Emission energy in water from ref 14. [d] Adiabatic approximation for vibronic coupling.

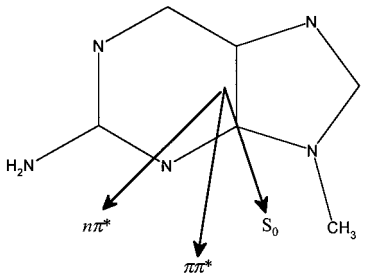

Figure 4. Permanent molecular dipole of 2A9MP in the ground (S_0), $\pi\pi^*$, and nπ^* states at the ground-state geometry. Length of arrows is proportional to dipole moment.

magnitude and direction of the excited-state dipoles are only weakly sensitive to the change in active space. At the ground-state geometry, the magnitudes of the dipoles are 3.6, 4.6, and 4.5 D for the ground, $\pi\pi^*$, and $n\pi^*$ states, respectively. The ground-state dipole is directed approximately along the C5−C4 bond. The $\pi\pi^*$ and $n\pi^*$ dipoles are rotated relative to the ground-state dipole in the direction of C2 by approximately −24° and −60°, respectively. At the $\pi\pi^*$ emitting geometry, the magnitudes of the dipoles are 3.7 and 4.3 D for the ground and $\pi\pi^*$ states, respectively. Relaxation of the excited state does not rotate these dipoles significantly from their orientation at the ground-state geometry.

The solvatochromic shift coefficients A and B (see Calculation Methods) for each of the electronic transitions discussed above are summarized in Table 4. On the basis of the molecular dipoles predicted by CASSCF, both the $\pi\pi^*$ absorption and emission spectra are predicted to shift to lower energy (longer wavelength) with increasing solvent polarity (or decreasing polarizability), with the magnitude of the shift being slightly greater for emission than for absorption. The weak dependence of the excitation energy on solvent properties arises from the small change (0.9 D) in dipole moment and orientation (24°) between the two states. For emission, the predicted spectral shift is slightly larger because the excited-state dipole is larger than that of the ground-state (see eq 2).

The calculated molecular dipoles were compared to experimental absorption and emission energies in a variety of solvents by performing a linear least-squares fit of eq 1 to the experimental spectral energies.[5,20,25] In this analysis, the cavity radius a and the vacuum transition energy E_0 were allowed to vary to maximize the agreement between calculated molecular dipoles and experimental energies. The experimental spectral maxima and lines of best fit are shown in Figure 5, and the recovered parameters are summarized in Table 4. Both absorption and emission energies are reasonably well predicted by eq 1, although the sensitivities of the two transitions to solvent differ markedly. Absorption spectra vary little in energy with solvent, while emission spectra undergo somewhat larger shifts. This difference is reflected in the best-fit parameters A/a^3 and

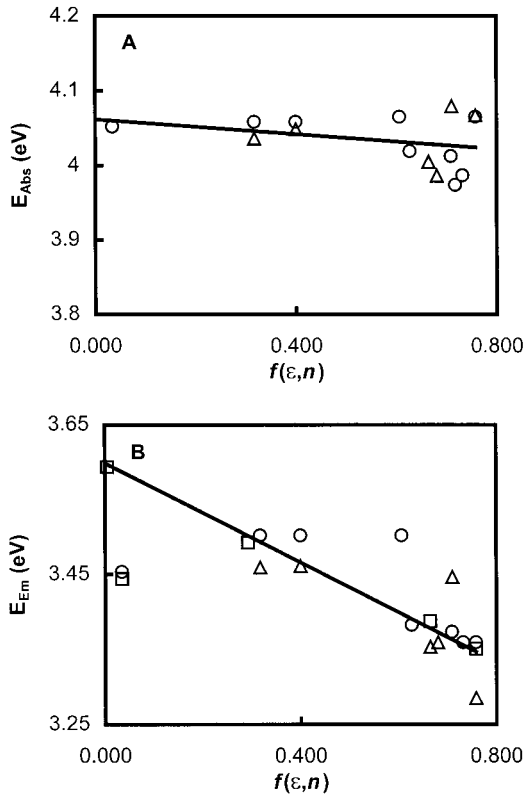

Figure 5. Least-squares fitting of eq 1 to the experimental absorption (A) and emission (B) spectral maxima from refs 9, (triangles), 13 (circles), and 14 (squares). The line represents the best fit of eq 1 to the experimental data; the parameters recovered from this analysis are summarized in Table 4. On the horizontal axis, $f(\epsilon,n)$ represents $(\epsilon - 1)/(\epsilon + 2) - (n^2 - 1)/(n^2 + 2)$, i.e., the factor multiplied by A in eq 1.

B/a^3 (Table 4), which represent the slope (in energy units) of the dependence of spectral shifts on solvent properties. For $\pi\pi^*$ absorption, A/a^3 is −0.06 eV, while for emission it is −0.35 eV, reflecting the much greater variation in emission energies with solvent.

These differing sensitivities of the two transitions to solvent polarity are also evident in the very different values of a that are required to fit the computed molecular dipoles to experimental absorption (a = 2.91 Å) and emission (a = 1.87 Å) shifts. The optimal value of a should be the same for both absorption and emission shifts because the effective radius of the solvent cavity is unlikely to differ significantly between absorbing and emitting states. The disagreement between these values implies that there are inaccuracies in some or all of the computed dipoles and, by extension, in the corresponding electronic states. Of the various electronic states, those calculated at the emitting geometry are probably the least accurate because of the limitations of excited-state geometry optimization. At the present time, excited-state geometries can only be obtained by

CASSCF (or less expensive methods). Perturbation theory, which is known to greatly improve the accuracy of ground-state geometries, cannot be applied to excited-state optimization. Therefore, the optimized $\pi\pi^*$ geometry is only approximate and may not resemble the actual emitting geometry closely enough to give correct molecular dipoles for all electronic states (although it does give an accurate MCQDPT emission energy). Despite the inconsistency with experiment, it is likely that many features of the optimized $\pi\pi^*$ geometry correspond to those of the true emitting state. In particular, the buckling of the optimized $\pi\pi^*$ state at C6 is likely to be present in the true emitting geometry because it arises in response to the large changes in electron density upon $\pi\pi^*$ excitation (as discussed above).

Experimental measurements of solvatochromic shifts for 2AP have generally predicted a larger dipole change between the ground and $\pi\pi^*$ states ($1.6\ \text{D} \leq \Delta\mu \leq 3.8\ \text{D}$) than is observed here.[5,7,20] However, the analysis performed in these studies differs in several important regards from the one here. First, the predicted value of $\Delta\mu$ depends sensitively on the cavity radius a, which previous investigators have arbitrarily taken to be 3.8 Å. Second, the previous studies and the current work employ slightly different theoretical formalisms to predict solvation energies. The dipoles predicted will differ with the choice of solvation model, although either model can be acceptably fitted to the experimental data by adjustment of the parameter a. Finally, the previous studies based their estimation of dipoles only on the Stokes' shift (the energy gap between absorption and emission maxima). Such an analysis implicitly assumes that the molecular dipoles are identical at both absorption and emission geometries. However, neither the experimental spectral data nor the dipoles computed here agree with this assumption. Therefore, it is difficult to compare the calculated molecular dipoles with those estimated by previous investigators directly. Nevertheless, the direction and relative magnitude of solvent-induced shifts in absorption and emission spectra predicted here are consistent with experimental results.[5,20,25]

In experimental measurements of absorption spectra in various solvents, a number of anomalous spectral shifts have been observed.[5,20] These results are consistent with the weak solvent sensitivity predicted here but, furthermore, suggest that specific interactions are important determinants of the solvatochromism of this fluorophore. Of particular interest, the absorption spectrum in water is shifted to energies higher than those in many less polar solvents, suggesting that hydrogen bonding in aqueous solution may stabilize the ground state more effectively than the $\pi\pi^*$ state.[5,20]

The energy of $n\pi^*$ absorption is predicted to increase with increasing solvent polarity, as can be seen from the coefficients in Table 4. This destabilization of the $n\pi^*$ state by the solvent relative to the ground state arises from the rotation of the $n\pi^*$ dipole, approximately 60° and 35° relative to those of the ground and $\pi\pi^*$ states, respectively. Upon excitation, the rotation of the permanent dipole of the fluorophore will cause solvent dipoles that were equilibrated around the ground-state fluorophore to be oriented unfavorably around the $n\pi^*$ state. Thus, although the magnitudes of $\pi\pi^*$ and $n\pi^*$ permanent dipoles are similar, the two states have very different solvent sensitivities due to the difference in the relative orientation of those dipoles.

The rotation of the $n\pi^*$ permanent dipole could also underlie the dependence of the fluorescence quantum yield on solvent polarity. When solvent molecules are equilibrated around the chromophore in the $\pi\pi^*$ state, dipolar interactions will destabilize the $n\pi^*$ state relative to the $\pi\pi^*$ state in proportion to the polarity of the solvent. Because the efficiency of vibronic coupling depends approximately inversely on the energy gap between the states,[26] the vibronic coupling between the $\pi\pi^*$ and $n\pi^*$ states will decrease in polar solvents. Consequently, the quantum yield of $\pi\pi^*$ fluorescence will increase in such solvents.

The solvent dependence of fluorescence quenching of 2AP by vibronic coupling between $\pi\pi^*$ and $n\pi^*$ states has also been postulated to arise from destabilization ("blue-shift") of the $n\pi^*$ state due to hydrogen bonding in polar solvents.[20] Such destabilization is likely to arise due to the loss of electron density on N1 in the $n\pi^*$ state (Figure 3). This change will make N1 a weaker H bond acceptor and consequently decrease the stabilizing energy of a hydrogen bond at this position. However, the molecular dipoles predicted here suggest that general solvent effects may play at least as important a role as hydrogen bonding in determining the efficiency of vibronic coupling.

Conclusions

2AP has been widely utilized as a fluorescence probe for biophysical studies of DNA structure, dynamics, and interactions, but mechanistic models that describe the effects of intra- and intermolecular processes on its fluorescence properties have not been developed. To facilitate the development of such models, we have calculated the lowest-energy singlet $\pi\pi^*$ and $n\pi^*$ excited states of 2A9MP using CASSCF and MCQDPT. The predicted energies for electronic excitation and fluorescence emission agree well with experimental values. Using a simple classical formulation of solvent interactions, we have predicted the effects of solvent polarity and polarizability on these electronic transitions. The $\pi\pi^*$ state is stabilized relative to the ground state at both Franck−Condon and emitting geometries in polar solvents due to dipolar interactions, and consequently, the energies of both $\pi\pi^*$ excitation and emission are modestly reduced. In contrast, the $n\pi^*$ state is destabilized relative to both the ground and $\pi\pi^*$ states in polar solvents, and the energy of transitions to this state are increased significantly. This effect arises almost entirely due to reorientation of the molecular dipole in the $n\pi^*$ state relative to those of the other two states. Therefore, it is predicted that the efficiency of $\pi\pi^*$ fluorescence quenching by vibronic coupling to the $n\pi^*$ state will decrease with increasing solvent polarity, consistent with experimental measurements of fluorescence quantum yield in various solvents.[20,25] Thus, the observed dependence of fluorescence quantum yield on solvent polarity can be rationalized purely in terms of classical dipolar interactions (although the current results do not exclude the possibility of significant hydrogen bonding effects). We hypothesize that this intramolecular quenching pathway may also underlie the effects of DNA conformation on the quantum yield of incorporated 2AP. It is possible that the nonpolar environment experienced by the chromophore within the DNA helix contributes to the fluorescence quenching. Conformational changes that increase the exposure of the probe to the more polar aqueous environment would increase the quantum yield. An extreme example of this phenomenon is the dramatic increase in DNA-incorporated 2AP fluorescence upon binding to enzymes that "flip" the base out of the helix.[14] Thus, the sensitivity of 2AP to DNA conformation could arise from the dependence of its quantum yield on the polarity of its environment.

Acknowledgment. The authors gratefully thank Patrick Callis, John Jean, and Kathleen B. Hall for stimulating discus-

sions and Drs. Jean and Hall for providing us with a copy of a manuscript in press. Certain preliminary results of this work were presented at the Jabłoński Centennial Conference on Luminescence and Photophysics, Toruń, Poland, July 1998, and were printed in the proceedings of that meeting.[17] This work was supported by NIH grant CA63317.

References and Notes

(1) Broo, A. *J. Phys. Chem. A* **1998**, *102*, 526−531.
(2) Broo, A.; Holmén, A. *J. Phys. Chem. A* **1997**, *101*, 3589−3600.
(3) Callis, P. *Annu. Rev. Phys. Chem.* **1983**, *72*, 329.
(4) Chignell, D. A.; Gratzer, W. B. *J. Phys. Chem.* **1968**, *72*, 2934−2941.
(5) Evans, K.; Xu, D.; Kim, Y.; Nordlund, T. M. *J. Fluoresc.* **1992**, *2*, 209−216.
(6) Frey, M. W.; Sowers, L. C.; Millar, D. P.; Benkovic, S. J. *Biochemistry* **1995**, *34*, 9185−92.
(7) Gryczynski, I.; Kawski, A. *Bull. Acad. Polon. Sci. (Ser. Sci. Math. Astron. Phys.)* **1977**, *26*, 1189−1195.
(8) Harnden, M. R.; Jarvest, R. L.; Slawin, A. M. Z.; Williams, D. J. *Nucleosides Nucleotides* **1990**, *9*, 499−513.
(9) Hochstrasser, R. A.; Carver, T. E.; Sowers, L. C.; Millar, D. P. *Biochemistry* **1994**, *33*, 11971−9.
(10) Holmén, A.; Nordén, B.; Albinsson, B. *J. Am. Chem. Soc.* **1997**, *119*, 9, 3114−3121.
(11) Krauss, M.; Osman, R. *J. Phys. Chem. A* **1997**, *101*, 4117−4120.
(12) Kwiatkowski, J. S. *Acta Phys. Polon.* **1968**, *34*, 365−385; *Chem. Abstr.* **1968**, *71*, 26119.
(13) Lim, E. C. *J. Phys. Chem.* **1986**, *90*, 6770−6777.
(14) McCullough, A. K.; Dodson, M. L.; Scharer, O. D.; Lloyd, R. S. *J. Biol. Chem.* **1997**, *272*, 27210−7.
(15) McRae, E. G. *J. Phys. Chem.* **1957**, *61*, 562−567.
(16) Nakano, H. *J. Chem. Phys.* **1993**, *99*, 7983−7992.
(17) Rachofsky, E. L.; Ross, J. B. A.; Krauss, M.; Osman, R. *Acta Phys. Polon. A* **1998**, *94*, 735−748.
(18) Roos, B. O. The Multiconfiguration SCF Method. In *Methods in Computational Molecular Physics*; Diercksen, G. H. F., Wilson, S., Eds.; D. Reidel Publishing: Dordrecht, The Netherlands, 1983; pp 161−187.
(19) Schmidt, M. W.; Baldridge, K. K.; Boatz, J. A.; Elbert, S. T.; Gordon, M. S.; Jensen, J. J.; Koseki, S.; Matsunaga, N.; Nguyen, K. A.; Su, S.; Windus, T. L.; Dupuis, M.; Montgomery, J. A. *J. Comput. Chem.* **1993**, *14*, 1347−1363.
(20) Smagowicz, J.; Wierzchowski, K. L. *J. Luminesc.* **1974**, *8*, 210−232.
(21) Sowers, L. C.; Fazakerley, G. V.; Eritja, R.; Kaplan, B. E.; Goodman, M. F. *Proc. Natl. Acad. Sci. U.S.A.* **1986**, *83*, 5434−8.
(22) Stevens, W. J.; Basch, H.; Krauss, M. *J. Chem. Phys.* **1984**, *81*, 6026.
(23) Stivers, J. T.; Pankiewicz, K. W.; Watanabe, K. A. *Biochemistry* **1999**, *38*, 952−63.
(24) Sullivan, J. J.; Bjornson, K. P.; Sowers, L. C.; deHaseth, P. L. *Biochemistry* **1997**, *36*, 8005−12; *Chem. Abstr.* **1997**, *88*, 135895.
(25) Ward, D. C.; Reich, E.; Stryer, L. *J. Biol. Chem.* **1969**, *244*, 1228−37.
(26) Wassam, W. A., Jr.; Lim, E. C. *J. Chem. Phys.* **1978**, *68*, 433−454; *Chem. Abstr.* **1999**, 138629.